phys. stat. sol. (b) **152**, 237 (1995)

Subject classification: 78.66; S5.11; S12

Faculty of Applied Science, Twente University, Enschede[1])

SSHG of Uniaxial Molecules: Phenomena near Brewster's Angle

By

C. M. J. WIJERS and P. L. DE BOEIJ

(Received March 9, 1995; in revised form May 2, 1995)

The nonlinear optical behaviour of a crystalline adlayer of unidirectionally oriented macromolecules at a substrate is studied by means of the discrete dipole model. Polar and azimuthal dependence of the second harmonic pp-reflectance is investigated at the fundamental and second harmonic frequencies. The influence of the anisotropic linear properties of the adlayer turns out to be essential.

Das nicht-lineare optische Verhalten einer kristallinen Schicht von parallel orientierten Makromolekülen auf einem Substrat wird mit dem diskreten Dipol-Verfahren untersucht. Die polare und azimutale Abhängigkeit der zweiten harmonischen pp-Reflektanz wird für die Grundfrequenz und deren zweite Harmonische berechnet. Der Einfluß der anisotropen linearen Eigenschaften der Schicht ist entscheidend.

1. Introduction

Most studies in the field of surface second harmonic generation (SSHG) concentrate primarily on second harmonic behaviour and try to link the experimentally obtained results to the nonlinear optical parameters as directly as possible. In previous papers we have published how SSHG can be calculated within the framework of a discrete dipole description [1 to 3]. The attractive aspect of such a calculation is that it allows for a microscopic treatment of both fundamental and second harmonic frequency responses. In this paper we want to show how phenomena at these two frequencies are related in the case of macromolecules, with strongly uniaxial, nonlinear optical behaviour, at silicon surfaces. Although the method itself is general, specific examples will only be given with data approximating as closely as possible calix [4] arenes [4] and with realistic adlayer thickness (48 monolayers). For adlayers on top of centrosymmetric materials, like silicon, SSHG has an expressed sensitivity. At the fundamental frequency this sensitivity is revealed either indirectly in difference measurements/calculations or directly in phenomena near Brewster's angle. In this paper we will concentrate on the simultaneous fundamental and second harmonic frequency response near Brewster's angle.

2. Nonlinear Discrete Dipole Theory

The substrate is modelled as a cubic discrete dipole lattice with a lattice parameter of $0.5a$ and terminated by a (001) surface. The macromolecules are placed on top of this surface in monolayers, such that again a (001)-oriented cubic lattice results with lattice parameter

[1]) P.O. Box 217, NL-7500 AE Enschede, the Netherlands.

a (see Fig. 1). The number of monolayers is N_{Ad}. The molecule sites are on top of one of the substrate sites of the cubic bulk lattice. The substrate–molecule spacing is $0.75a$. The positive z-direction is along the surface normal and points towards the crystal interior. The incoming electromagnetic plane wave has the electric field $\boldsymbol{E}(\boldsymbol{r}, t)$,

$$\boldsymbol{E}(\boldsymbol{r}, t) = E_0 \hat{\boldsymbol{e}} \exp\left(i[\boldsymbol{k}\boldsymbol{r} - \omega_0 t]\right), \tag{1}$$

with amplitude E_0 and polarisation direction $\hat{e}$. The wave vector is $\boldsymbol{k}$ and the frequency ω_0. The angle between $\boldsymbol{k}_{\|}$, the projection of $\boldsymbol{k}$ onto the surface, and one of the surface crystallographic directions is the anisotropic azimuth Ω. The angle of incidence is θ_i. The nonlinear induction has to be written in the frequency domain as

$$\boldsymbol{p}(\omega) = \boldsymbol{\alpha}(\omega)\, \boldsymbol{E}_L(\omega) + \int_{-\infty}^{\infty} d\omega'\, \boldsymbol{\beta}(\omega', \omega - \omega')\, \boldsymbol{E}_L(\omega')\, \boldsymbol{E}_L(\omega - \omega'). \tag{2}$$

This equation acts as a generator for the induction at fundamental and second harmonic frequencies, when a monochromatic beam (1) is used. Representing this monochromatic beam as a superposition of delta-functions in frequency space, the characteristic dipole $\boldsymbol{p}_i$ for plane i [5] gets induced by the local field $\boldsymbol{E}_i^L$, as

$$\begin{aligned} \boldsymbol{p}_i(\omega_0) &= \boldsymbol{\alpha}_i(\omega_0)\, \boldsymbol{E}_i^{L*}(\omega_0) + 2\boldsymbol{\beta}_i(-\omega_0, 2\omega_0)\, \boldsymbol{E}_i^{L*}(\omega_0)\, \boldsymbol{E}_i^L(2\omega_0), \\ \boldsymbol{p}_i(2\omega_0) &= \boldsymbol{\alpha}_i(2\omega_0)\, \boldsymbol{E}_i^L(2\omega_0) + \boldsymbol{\beta}_i(\omega_0, \omega_0)\, \boldsymbol{E}_i^L(\omega_0)\, \boldsymbol{E}_i^L(\omega_0), \end{aligned} \tag{3}$$

where $\boldsymbol{\alpha}_i$ is the polarisability tensor and $\boldsymbol{\beta}_i$ the hyperpolarisability tensor, for which we will use the symmetry relations of the corresponding nonlinear susceptibilities. In (3), we have

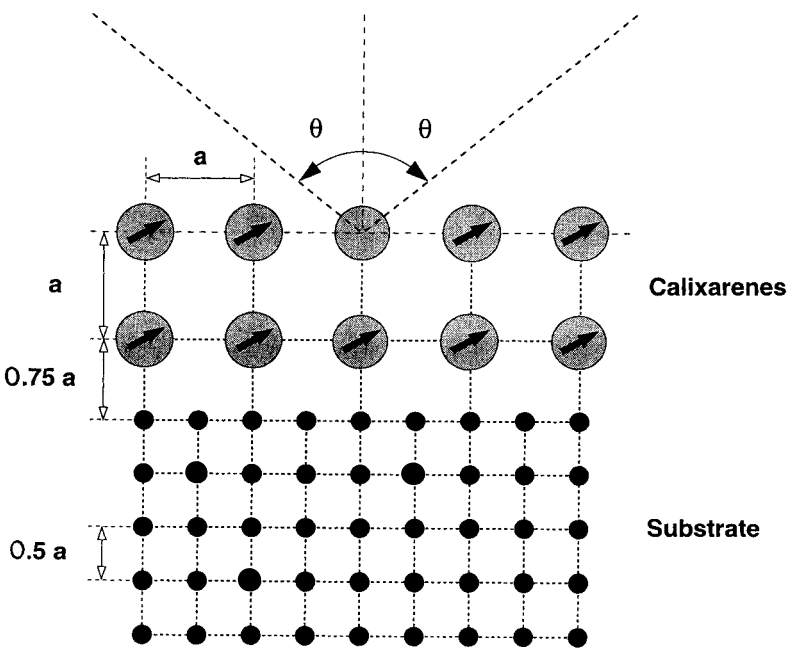

Fig. 1. Monolayers of calixarenes on silicon: model configuration

omitted the contribution of the (very weak) radiation damping. Further in this paper we will not distinguish between ω_0 and ω and will use only ω. The last term of the first line of (3) introduces the beam depletion, whereas the first term in the second line of this equation describes the local field effect at the second harmonic frequency. Simultaneous solution of the set of nonlinear coupled equations (3) is performed by iteration, resulting in a succession of linear steps. Then we have to define the auxiliary down-converting vector $\boldsymbol{E}_j^{\mathrm{down},n}$ and up-converting vector $\boldsymbol{E}_j^{\mathrm{up},n}$, consisting of the nonlinear parts of (3) and given for the n-th step by

$$\begin{aligned} \boldsymbol{E}_i^{\mathrm{down},n}(\omega) &= 2\boldsymbol{\alpha}_j^{-1}(\omega)\,\boldsymbol{\beta}_j(\omega)\,\boldsymbol{E}_{\mathrm{L},i}^n(2\omega)\,\boldsymbol{E}_{\mathrm{L},i}^n(\omega)^*\,, \\ \boldsymbol{E}_i^{\mathrm{up},n}(2\omega) &= \boldsymbol{\alpha}_j^{-1}(2\omega)\,\boldsymbol{\beta}_j(2\omega)\,\boldsymbol{E}_{\mathrm{L},i}^n(\omega)\,\boldsymbol{E}_{\mathrm{L},i}^n(\omega)\,. \end{aligned} \tag{4}$$

For the local fields $\boldsymbol{E}_{\mathrm{L},i}^n(\omega)$ the following explicit expression has been used [5]:

$$\boldsymbol{E}_{\mathrm{L},i}^n(\omega) = \boldsymbol{E}_0 \exp(i\boldsymbol{k}\boldsymbol{r}_i) + \alpha_0^{-1} \sum_{i \neq j} f_{ij}(\omega)\,\boldsymbol{p}_j^n(\omega)\,, \tag{5}$$

where the external field $\boldsymbol{E}_0 \exp(i\boldsymbol{k}\boldsymbol{r}_i)$ is zero for the second harmonic frequency. For the iterative solution we suppose that the nonlinear contributions (4) are known from the previous step. As a result we obtain two sets of linear equations, which for crystalline surfaces can be solved by means of the double cell method [5, 1] in a numerically efficient way. For a full description of this method and the meaning of some variables the reader is referred to [5, 6]. We need further the bulk dipole strengths, written as normal modes,

$$\boldsymbol{p}_{vV} = \sum_{m=1}^{M} v_m \boldsymbol{u}_{mv}\, \mathrm{e}^{iq_m V d_{\mathrm{B}}}\,, \tag{6}$$

where $\boldsymbol{p}_{vV}$ is the dipole strength belonging to site v of the V-th bulk unit cell, having height d_{B}. The quantities $\boldsymbol{u}_{mv}$, the normal mode eigenvector, and q_m, the normal mode wave number, are completely determined by the bulk. Here we have to assume that the behaviour of the bulk is linear. Only the normal mode strength, v_m, can be affected by phenomena taking place in the surface region and nonlinearity can only be taken into account for the adlayer.

The results for step $(n + 1)$ for the fundamental frequency follow from

$$\begin{Vmatrix} \mathscr{M}_{\mathrm{SS}}(\omega) & \mathscr{M}_{\mathrm{SB}}(\omega) \\ \mathscr{M}_{\mathrm{BS}}(\omega) & \mathscr{M}_{\mathrm{BB}}(\omega) \end{Vmatrix} \begin{vmatrix} \boldsymbol{p}_j^{n+1}(\omega) \\ v_m^{n+1}(\omega) \end{vmatrix} = \begin{vmatrix} \boldsymbol{E}_i(\omega) + \boldsymbol{E}_i^{\mathrm{down},n}(\omega) \\ \mathscr{E}_t(\omega) \end{vmatrix}, \tag{7}$$

where $\boldsymbol{E}_i(\omega)$ is the external field for a characteristic (surface) site $\boldsymbol{r}_i$, as given by (1), and $\mathscr{E}_t(\omega)$ the projection of the amplitude $E_0\hat{\boldsymbol{e}}$ onto $\hat{\boldsymbol{t}}$. The unit vector $\hat{\boldsymbol{t}}$ corresponds to either s- or p-polarised input. For the second harmonic frequency we have to use

$$\begin{Vmatrix} \mathscr{M}_{\mathrm{SS}}(2\omega) & \mathscr{M}_{\mathrm{SB}}(2\omega) \\ \mathscr{M}_{\mathrm{BS}}(2\omega) & \mathscr{M}_{\mathrm{BB}}(2\omega) \end{Vmatrix} \begin{vmatrix} \boldsymbol{p}_j^{n+1}(2\omega) \\ v_m^{n+1}(2\omega) \end{vmatrix} = \begin{vmatrix} \boldsymbol{E}_j^{\mathrm{up},n+1}(2\omega) \\ 0 \end{vmatrix}. \tag{8}$$

The matrices $\mathscr{M}_{\mathrm{SS}}$, $\mathscr{M}_{\mathrm{SB}}$, $\mathscr{M}_{\mathrm{BS}}$, and $\mathscr{M}_{\mathrm{BB}}$, do not depend on iteration and the effort required to do the iteration is relatively modest as compared to linear double cell calculations. The subscripts S and B refer to surface or bulk, respectively. The detailed expressions for the matrix elements of the sub-matrices shown in (7), (8) can be found in [5].

The iteration process has to be started by assuming for the first step that

$$\boldsymbol{E}_j^{\text{down},0} = 0\,. \tag{9}$$

If convergence has been obtained in the iteration process to within the required numerical accuracy, we have solved the nonlinear set (7), (8). Then for fundamental and second harmonic frequencies the sources $(\boldsymbol{p}_i, v_m)$ are available. From these the reflection coefficient r_t can be obtained for both frequencies by means of

$$r_t = \frac{2\pi i a^3 k^2}{\mathscr{S}\,|k_z|}\left[\frac{\hat{\boldsymbol{t}}\cdot\left(\sum_{j=1}^{\infty} \mathrm{e}^{-i\boldsymbol{k}\boldsymbol{r}_j}\,\boldsymbol{p}_j\right)}{\alpha_0 E_0}\right], \tag{10}$$

where the dipole strengths for the bulk region have to be obtained from the explicit normal mode expressions, as given by (6), $\mathscr{S}$ is the area of the surface unit cell and $\alpha_0 = 4\pi\varepsilon_0 a^3$. Further $\boldsymbol{k}$ is the reflected wave vector and $\hat{\boldsymbol{t}}$ corresponds to either s- or p-polarised output. Equation (10) connects directly microscopic and macroscopic responses.

3. Numerical Results

The square lattice of macromolecules has the lattice parameter $a = 1$ nm. The fundamental frequency has been assumed as $\hbar\omega = 1.165$ eV of a Nd:YAG laser and $E_0 = 10^7$ V/m. The linear polarisabilities of the silicon substrate have been derived from the Clausius-Mossotti relation using a dielectric constant of 12.466 for the fundamental and $17.2241 + i0.4296$ for the second harmonic frequency. The nonlinear behaviour of the macromolecules is taken uniaxial [4], with $\beta_{zzz} = 1.11 \times 10^{-49}$ Fm^3/V. The average linear behaviour of the macromolecules corresponds to the average polarisability $\bar{\alpha}$ and follows from refractive indices $n(1) = 1.565$ and $n(2) = 1.535$ through the Clausius-Mossotti relation.

In our previous paper [3], we have studied almost exclusively cases with isotropic linear behaviour of the macromolecules. Isotropic behaviour is not consistent with experiment [7] and simultaneous isotropic linear behaviour and uniaxial nonlinear behaviour of macromolecules can hardly be understood theoretically. For this reason we focus in this paper also upon the influence of linear anisotropy. All (hyper)polarisabilities will be defined in the molecular frame of axes (M). Keeping the trace of the polarisability tensor constant, the polarisability is made anisotropic through

$$\alpha_{zz}^{\mathrm{M}} = r_{\mathrm{Ani}}\alpha_{xx}^{\mathrm{M}} = r_{\mathrm{Ani}}\alpha_{yy}^{\mathrm{M}}\,, \tag{11}$$

where r_{Ani} is the anisotropy ratio. For all cases to be treated in this paper we will use a constant linear anisotropy of $r_{\mathrm{Ani}} = 7.0$. This value is just a guess for the calix molecules, since there are no experimental data for this parameter. Rotation of the molecule to the laboratory frame (L), starting from a molecular orientation along the z-axis, is taken into account by rotating the (hyper)polarisabilities according to [8],

$$\alpha_{pq}^{\mathrm{L}}(\theta_{\mathrm{M}}) = \sum_{i,j} S_{pi}\alpha_{ij}^{\mathrm{M}}(S^{-1})_{jq}\,, \tag{12}$$

$$\beta_{pqr}^{\mathrm{L}}(\theta_{\mathrm{M}}) = \sum_{i,j,k} S_{pi}\beta_{ijk}^{\mathrm{M}}(S^{-1})_{jq}\,(S^{-1})_{kr}\,. \tag{13}$$

All adsorbed macromolecules rotate in the xz-plane over the same angle θ_{M} with respect to the surface normal and S is the rotation matrix. The tilt will always be directed towards

the positive x-axis. In this paper we consider only pp-type reflectances since we are interested here in phenomena near Brewster's angle, for reasons of (linear) surface sensitivity.

In optical applications using macromolecules, precise knowledge of their properties is required. In situ characterisation, as studied in this paper, yields then more relevant information. The model calculations in this paper are controlled by only seven key parameters, a, N_{Ad}, $\bar{\alpha}$, r_{Ani}, θ_{M}, E_0, and β_{zzz}, when we assume that the substrate properties are known. The more macromolecule parameters can be determined independently by other methods, the easier it becomes to find the remaining ones. Clausius-Mossotti type calculations yield only the value for $\bar{\alpha}/a^3$, so a unique value for $\bar{\alpha}$ is only obtained for given a. This lattice parameter a has to be known from other sources. This holds also for the number of monolayers in the adlayer N_{Ad}. The three parameters a, N_{Ad}, and $\bar{\alpha}$ control the overall quantitative linear optical properties of the adlayer/substrate system. The shape of the linear response becomes determined by the parameters r_{Ani} and θ_{M}. These control the shape of the azimuthal plots near Brewster's angle, but also other linear optical properties, as difference and/or ellipsometric measurements, can be used to isolate these two parameters. The parameters left are E_0 and β_{zzz}. Since beam depletion is weak, a single step in the iteration yields already the major information. Then from the inhomogeneous term in (8) a factor $E_0^2\beta_{zzz}$ can be extracted and the remainder controls the shape, completely determined by the already obtained parameters. Hence from SSHG one can only obtain the factor $(E_0^2\beta_{zzz})^2$ and the shape information has to be in agreement with the linear data. To learn about the absolute strength of β_{zzz} requires the value of E_0, which has to be measured independently.

The advantage of a microscopic discrete dipole calculation, is easy access to the microscopic source terms, i.e. the individual dipole strengths. Those have been shown in Fig. 2, where we have used isotropic macromolecules ($r_{\mathrm{Ani}} = 1.0$), with molecular axis perpendicular to the surface ($\theta_{\mathrm{M}} = 0°$). In studying this figure one fact has to be taken into account. Only contributions of equal volumes can be compared. Since the spacing of the substrate lattice is half the spacing of the adlayer lattice, the combined contribution of eight bulk dipoles needs to be compared with a single surface dipole. This brings bulk and surface dipole strengths effectively within the same order of magnitude. At the fundamental frequency no influence of an increased thickness of the adlayer on the bulk dipole strengths can be observed. For the second harmonic frequency two facts are remarkable. First, there is a bulk response, and second, this response depends on the adlayer thickness. In classical continuum descriptions, symmetry forbids the occurrence of a nonzero nonlinear susceptibility. For the same reason we have assigned only linear polarisabilities to the bulk. Despite that we find nonzero second harmonic dipole strengths in the bulk. The explanation can be found in the second line of (3) and is straightforward. For this type of calculations the second harmonic local field $\boldsymbol{E}_i^{\mathrm{L}}(2\omega_0)$ is nonzero, since the adlayer produces second harmonic radiation, emits it to the substrate and causes there, through linear induction, a nonzero second harmonic dipole strength $\boldsymbol{p}_i(2\omega_0)$. So the primary source of this second harmonic bulk effect is in the adlayer, and this explains the dependence on the adlayer thickness.

Brewster's minima can be found from calculations dependent on the angle of incidence (polar plots). In Fig. 3a we show the polar plot of the reflectance for the fundamental frequency. The curves turn out to be always perfectly symmetric, also when the macromolecules are tilted. The position of Brewster's minimum is rather precisely at 74°. The calculated curves depend only weakly on the tilt angle of the molecules, despite the 48 monolayers in the adlayer. In Fig. 3b the corresponding second harmonic reflectance, defined

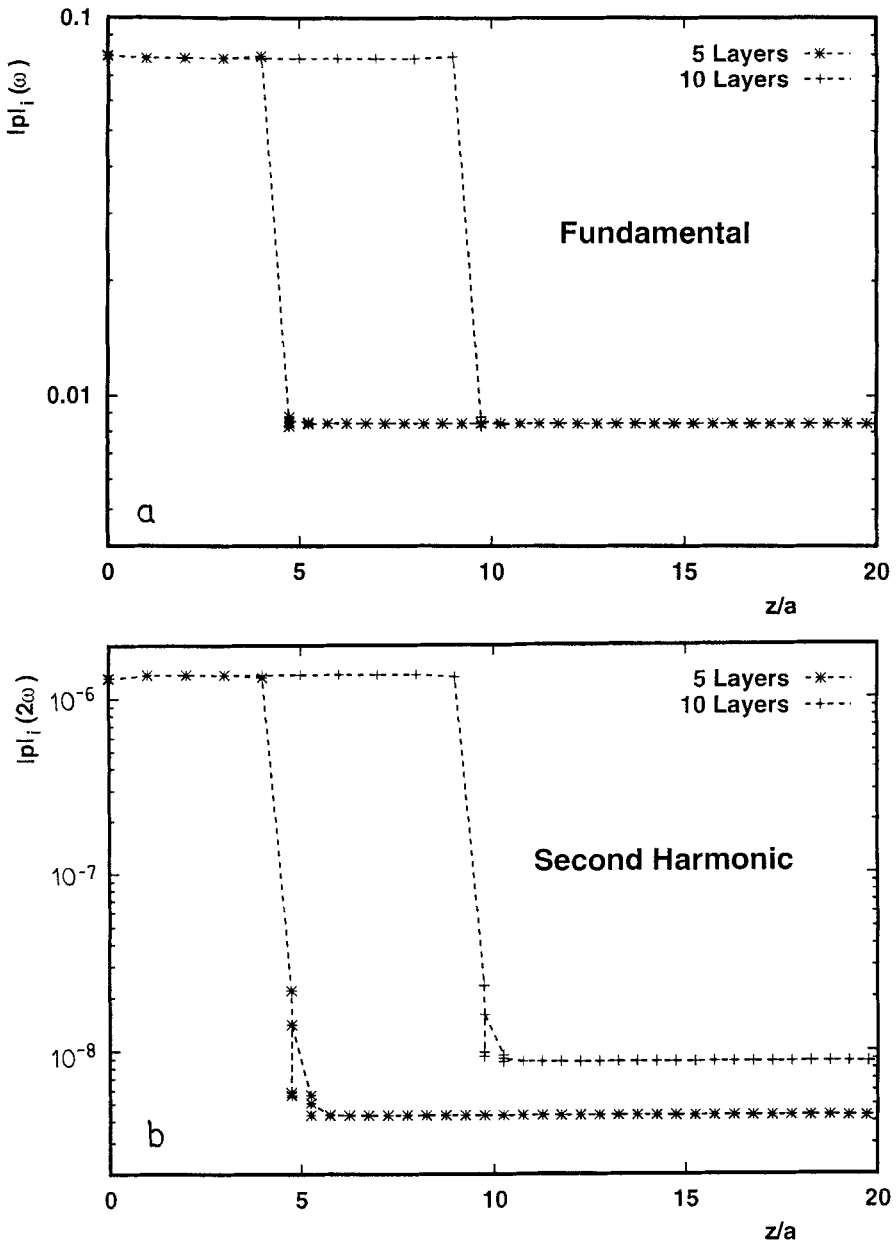

Fig. 2. Modulus of dipole strength as a function of z-coordinate, $\theta_i = 45°$ and $\theta_M = 0°$

as second harmonic reflected intensity divided by the fundamental frequency incoming intensity, is shown. The reference for the second harmonic curves is that for $\theta_M = 72°$. For this tilt of the molecule a minimum in the pp-response is found being close to 74°, the linear Brewster's angle. It is remarkable to see how far the molecule had to be tilted in order to produce that minimum. For the linearly isotropic cases studied in [3] we found

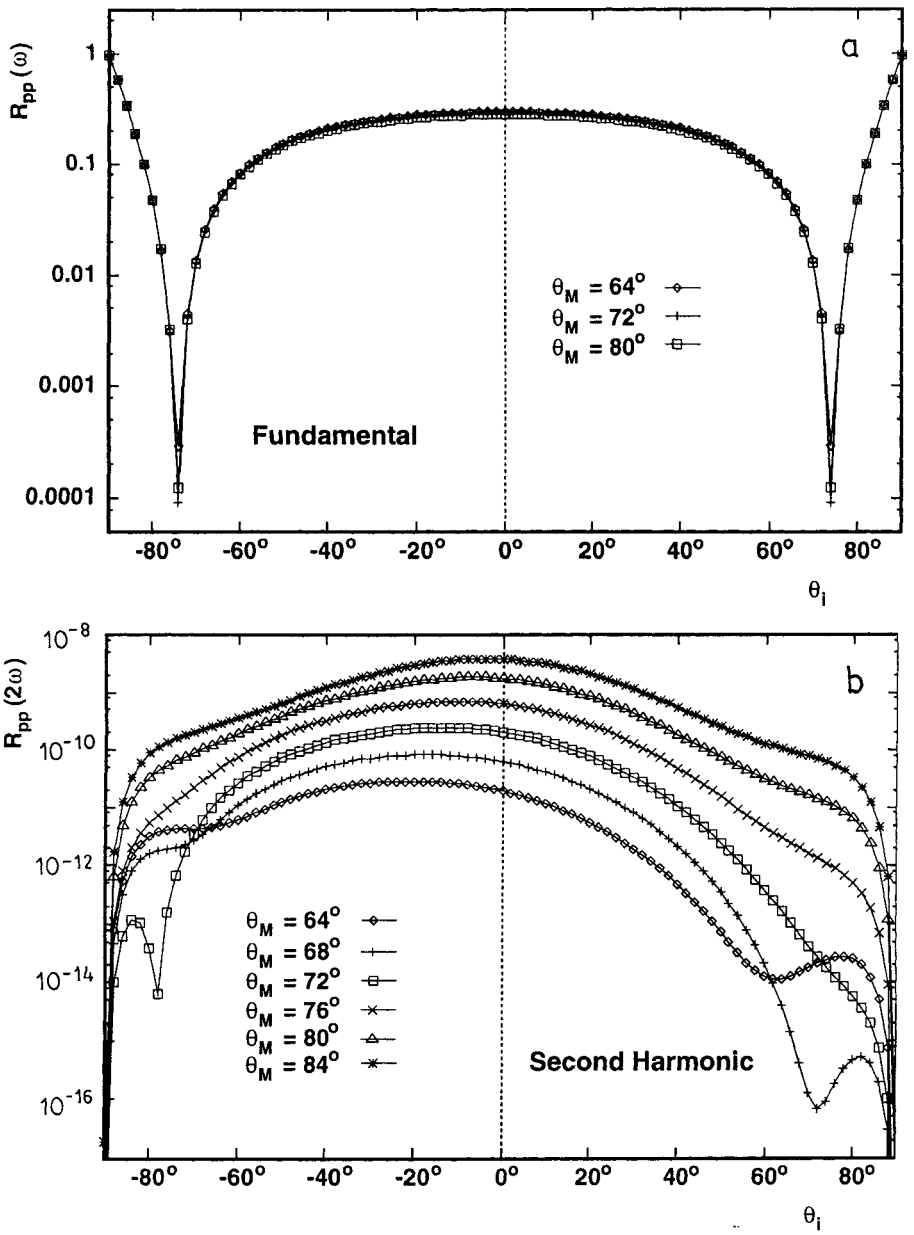

Fig. 3. pp-type reflectance as a function of θ_i for $\Omega = 0°$ and 48 layers of calix at several high values of θ_M

much lower tilt angles ($\theta_M = 30°$) to produce a minimum at $\theta_i \approx 55°$. From (4), (8) we can conclude that for $\boldsymbol{E}^n_{L,i}(\omega)$ at right angles with the axis of the molecule, no second harmonic sources can be produced and the second harmonic reflection has to be zero. For linearly isotropic molecules, dipole strength and local field are parallel, but the dipole strength itself is also nearly perpendicular to the refracted beam in the adlayer [5]. If the second harmonic

minimum has to coincide with Brewster's minimum, it is simple to calculate that θ_M has to be about 37° for linearly isotropic molecules. The corresponding second harmonic minimum for anisotropic cases was found to be at $\theta_M = 72°$. The large discrepancy between the two values of θ_M can only be due to the linear anisotropy, particularly the fact that local field and dipole strength are no longer automatically parallel. All second harmonic curves are highly asymmetric and if there are minima, they are not as pronounced as for the fundamental frequency. When the local field is perpendicular to the molecular axis, the sharp minimum is obtained. The other second harmonic shallow minimum is the result of (10) and can be explained in the same way, as we did for Brewster's minimum in [5]. For higher tilt angles the overall intensity increases, whereas the asymmetry decreases.

We will concentrate in the remainder of this paper upon the behaviour of azimuthal curves (all azimuthal curves to be shown will have the same orientation, i.e. horizontal axis along the x-direction), because they are best accessible for experimentalists. For three angles near Brewster's minimum, $\theta_i = 72°, 74°$, and 76° we have calculated azimuthal curves for a tilt angle of 72°. As was to be expected from the results of Fig. 3 the fundamental frequency curves are strongly dependent on θ_i. Second harmonic frequency results depend only weakly on the angle of incidence. For the fundamental frequency our interest concerns primarily features which depend on the linear anisotropy and the tilt angle of the macromolecules. The azimuthal pp-type plots are in general isotropic. Only very close to Brewster's angle strong anisotropy can be found. The second harmonic plots shown in Fig. 4b show a pattern with two lobes and the beginning of a three-lobe pattern. These types of pattern have been found also for the case of linearly isotropic monolayers [3] and calculations confirm that also for thicker anisotropic adlayers no pattern of fundamentally different character will be observed in the second harmonic plots.

For the constant value of linear anisotropy $r_{Ani} = 7.0$ assumed in this paper, we have calculated a number of azimuthal plots at the 74° Brewster's minimum, for values of θ_M around 72°. Results are shown in Fig. 5. Fig. 5b are the second harmonic results. The different curves are well suited to distinguish between several tilt angles of the molecule. Important is the curve at $\theta_M = 76°$, having a four-lobe shape. All curves for higher angles have the same type of two-lobe shape, only the relative difference in size between left and right changes, until finally the two lobes will be of the same size for $\theta_M = 90°$. In view of the preliminary experimental data about single domains of calixarenes [7], the likely shape is that at about $\theta_M = 84°$. For this reason we have calculated more cases for θ_M above than for θ_M below 72°. Fig. 5a shows the fundamental frequency results. Also these curves are clearly different for several values of the tilt angle. They all have the symmetric shape characteristic of linear response. Remarkable are the curves for $\theta_M = 76°$, 80°, and 84°. They have an unexpected four-lobe structure. In order to learn more about the possible reasons of these peculiar structures, we made some additional calculations.

For $\theta_M = 84°$ we investigated four cases. First we wanted to investigate, whether perhaps the four-lobe patterns originate from the beam depletion. Calculations with $E_0 = 10^7$ and 0 V/m revealed only differences in the seventh digit, so this option can be forgotten. Next we have investigated three linear cases, results being show in Fig. 6. This figure displays the results for a bare silicon substrate as used in these calculations, and results for two different adlayers consisting of 48 layers of calix. The first being for linearly isotropic calix and the second for linearly anisotropic calix with $r_{Ani} = 7.0$. The only anisotropic curve is the curve for anisotropic calix. Both other cases are perfectly isotropic. So the conclusion has to be that deviation from isotropy, including the remarkable four-lobe pat-

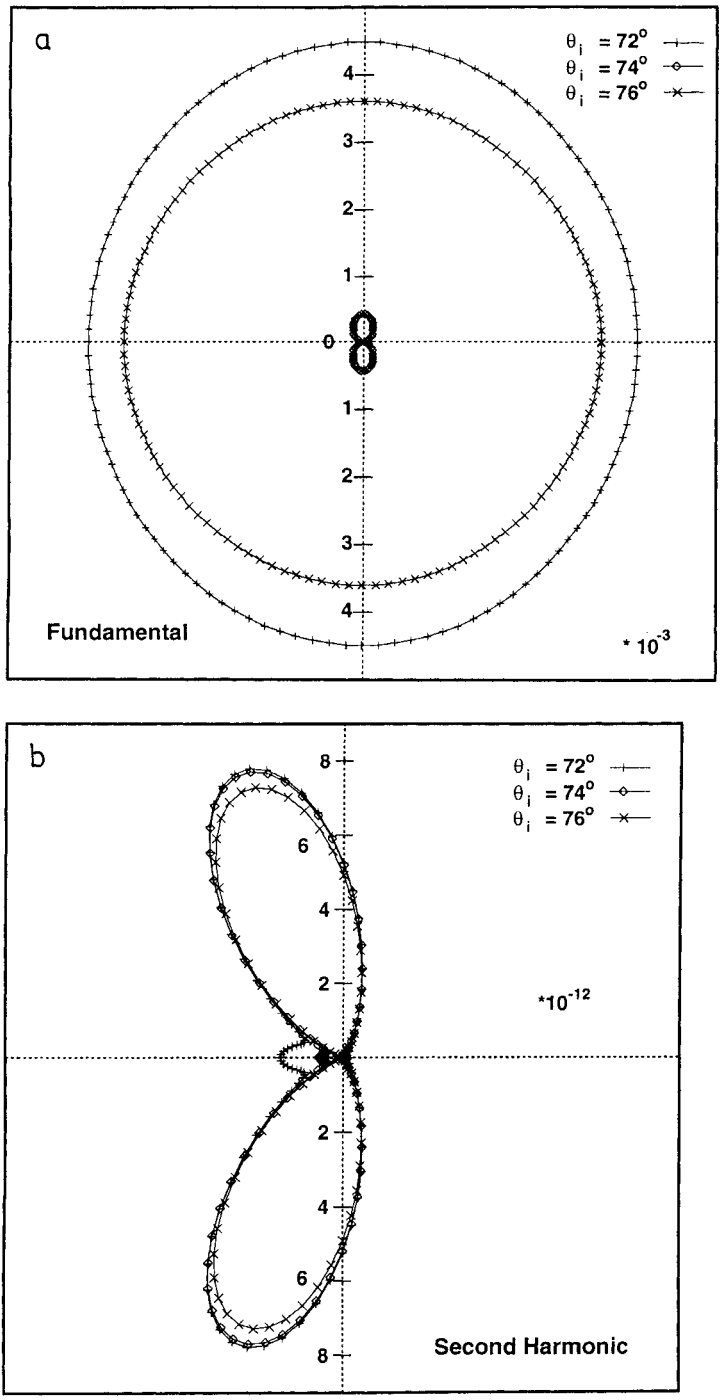

Fig. 4. pp-type reflectance as a function of Ω for $\theta_M = 72°$ and 48 layers of calix at several values of θ_i near Brewster's angle

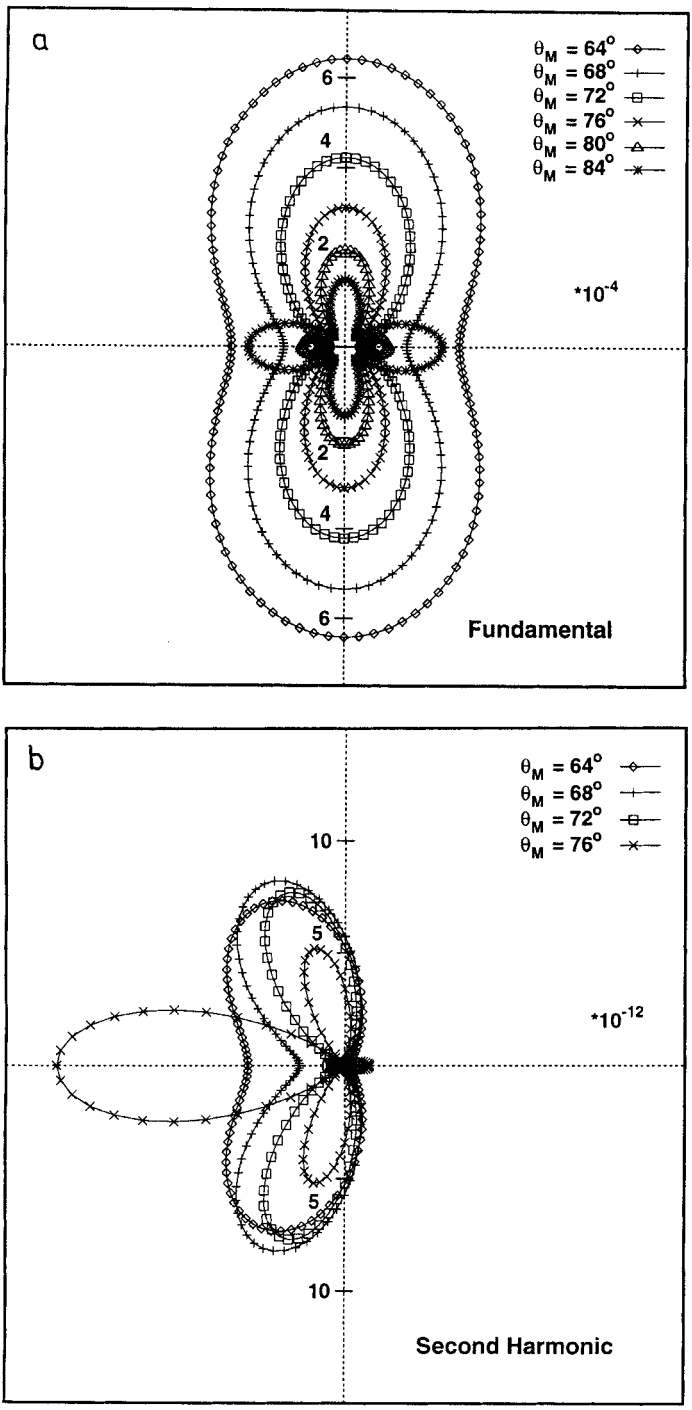

Fig. 5. pp-type reflectance as a function of Ω for $\theta_i = 74°$ and 48 layers of calix at several values of θ_M

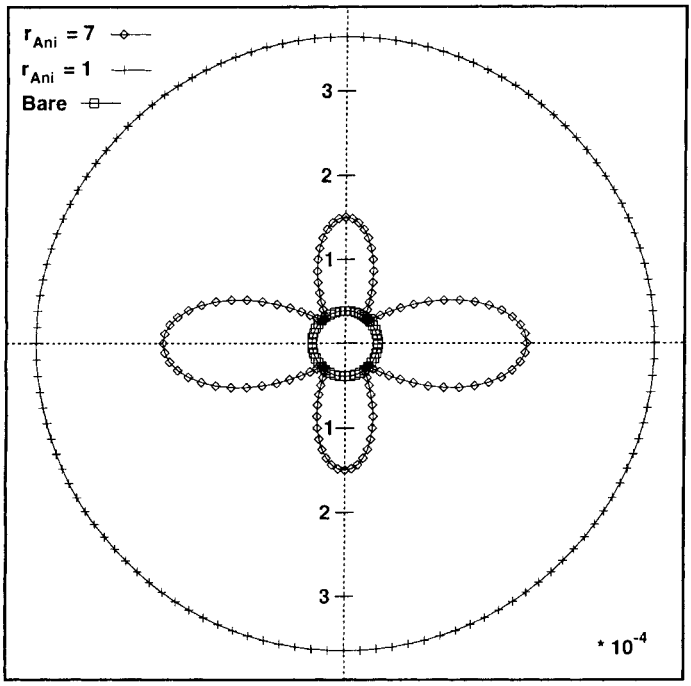

Fig. 6. pp-type reflectance as a function of Ω for $\theta_i = 74°$, $\theta_M = 84°$. Bare Si, 48 layers $r_{Ani} = 1.0$, and 48 layers $r_{Ani} = 7.0$

terns, is controlled only by the anisotropy of the macromolecules of the adlayer. This holds for linear cases and for the fundamental and second harmonic frequencies of nonlinear cases.

4. Conclusions

In this paper we have studied the linear and nonlinear optical properties of uniaxial molecules on surfaces, using values approximating calix [4] arenes, to support ongoing (experimental) research in that field. Nonlinear optical behaviour has been reported in the literature for other macromolecule/surface systems, like p-nitrophenol, rhodamine dyes, and several types of liquid crystal, as can be found in a recent review [9]. The SSHG by liquid crystals, especially the azimuthal plots obtained from rubbed films, are particularly relevant for this paper. Those results have been obtained by Barmentlo and coworkers [10, 11] and their pp-results for strongly rubbed films are in good agreement with the $\theta_M = 84°$ results of this paper. Linear optical properties of the macromolecules strongly influence the second harmonic response. This holds particularly for the anisotropic response, which depends, as shown in this paper, on both the linear and nonlinear tensor anisotropies. In view of these results a careful analysis of the linear properties of these molecules is essential. The fundamental frequency pp-response near Brewster's angle shows a sensitivity for the optical properties of the adlayer, comparable with SSHG itself. A unique determination of the single nonzero component of the molecular hyperpolarisability is only possible if the linear molecular data are known. These should preferably be obtained from more traditional linear measurements, like e.g. differential ellipsometric or comparable measurements.

References

[1] C. M. J. WIJERS, TH. RASING, and R. W. J. HOLLERING, Solid State Commun. **85**, 233 (1993).
[2] C. M. J. WIJERS, R. LANTINGA, and N. F. VAN HULST, Proc. CLEO/Europe EQEC'94 (1994), IEEE Catalog Number 94TH0615-5, IEEE Service Center, Piscataway (NJ, USA).
[3] C. M. J. WIJERS, R. LANTINGA, and P. L. DE BOEIJ, Surface Sci. **331/333**, 1329 (1995).
[4] G. J. T. HEESINK, A. G. T. RUITER, N. F. VAN HULST, and B. BÖLGER, Phys. Rev. Letters **71**, 999 (1993).
[5] C. M. J. WIJERS and G. P. M. POPPE, Phys. Rev. B **46**, 7605 (1992).
[6] G. P. M. POPPE, C. M. J. WIJERS, and A. VAN SILFHOUT, Phys. Rev. B **44**, 7917 (1991).
[7] N. F. VAN HULST, private communication.
[8] R. BERSOHN, Y. PAO, and H. L. FRISH, J. chem. Phys. **45**, 3184 (1966).
[9] R. M. CORN and D. A. HIGGINS, Chem. Rev. **94**, 107 (1994).
[10] M. BARMENTLO, N. A. J. M. VAN AERLE, R. W. J. HOLLERING, and J. P. M. DAMEN, J. appl. Phys. **71**, 4799 (1992).
[11] N. A. J. M. VAN AERLE, M. BARMENTLO, and R. W. J. HOLLERING, J. appl. Phys. **74**, 3111 (1993).